Synthesis of Error-Recovery Protocols for Micro-Electrode-Dot-Array Digital Microfluidic Biochips

MAHMOUD ELFAR, ZHANWEI ZHONG, ZIPENG LI, KRISHNENDU CHAKRABARTY, and MIROSLAV PAJIC, Duke University

A digital microfluidic biochip (DMFB) is an attractive technology platform for various biomedical applications. However, a conventional DMFB is limited by: (i) the number of electrical connections that can be practically realized, (ii) constraints on droplet size and volume, and (iii) the need for special fabrication processes and the associated reliability/yield concerns. To overcome the above challenges, DMFBs based on a micro-electrode-dot-array (MEDA) architecture have been proposed and fabricated recently. Error recovery is of key interest for MEDA biochips due to the need for system reliability. Errors are likely to occur during droplet manipulation due to defects, chip degradation, and the uncertainty inherent in biochemical experiments. In this paper, we first formalize error-recovery objectives, and then synthesize optimal error-recovery protocols using a model based on Stochastic Multiplayer Games (SMGs). We also present a global error-recovery technique that can update the schedule of fluidic operations in an adaptive manner. Using three representative real-life bioassays, we show that the proposed approach can effectively reduce the bioassay completion time and increase the probability of success for error recovery.

CCS Concepts: • **Computer systems organization → Embedded software**; *System on a chip*; • **Mathematics of computing** → *Markov processes*; • **Theory of computation** → *Formalisms*;

Additional Key Words and Phrases: Digital microfluidics, controller synthesis, lab-on-chip, micro-electrode-dot-array (MEDA), formal methods, stochastic games

ACM Reference format:
Mahmoud Elfar, Zhanwei Zhong, Zipeng Li, Krishnendu Chakrabarty, and Miroslav Pajic. 2017. Synthesis of Error-Recovery Protocols for Micro-Electrode-Dot-Array Digital Microfluidic Biochips. *ACM Trans. Embed. Comput. Syst.* 16, 5s, Article 127 (September 2017), 22 pages.
https://doi.org/10.1145/3126538

1 INTRODUCTION

Digital microfluidics enables the manipulation of droplets of picoliter volumes under program control based on the principle of electrowetting-on-dielectric (EWOD) [10]. Digital microfluidic

This work was supported in part by the NSF CNS-1652544 and CNS-1505701 grants, and the Intel-NSF Partnership for Cyber-Physical Systems Security and Privacy.
This article was presented in the International Conference on Compilers, Architecture, and Synthesis for Embedded Systems (CASES) 2017 and appears as part of the ESWEEK-TECS special issue
Authors' addresses: M. Elfar, Z. Zhong, Z. Li, K. Chakrabarty, and M. Pajic, Hudson Hall, 100 Science Drive, Department of Electrical and Computer Engineering, Duke University, Durham, NC 27708, USA; emails: {mahmoud.elfar, zhanwei.zhong, zipeng.li, krishnendu.chakrabarty, miroslav.pajic}@duke.edu.

https://doi.org/10.1145/3126538

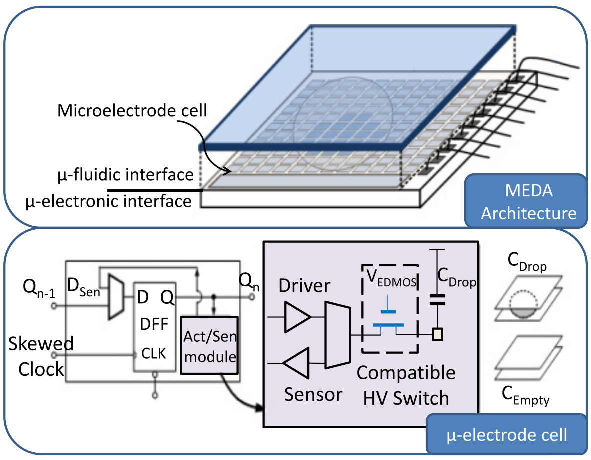

Fig. 1. Illustration of the MEDA architecture and microelectrode cell (μ-electrode cell) [16].

biochips (DMFBs) are revolutionizing point-of-care diagnostics [20], high-throughput DNA sequencing [23], drug discovery [2], and environmental toxicity monitoring [6]. However, today's DMFBs suffer from several limitations, mainly: (i) inability to vary droplet volume in a fine-grained manner, (ii) the lack of integrated sensors for real-time detection, and (iii) the need for special fabrication processes and the associated reliability/yield concerns. To overcome the above limitations, a micro-electrode-dot-array (MEDA) architecture has been proposed recently [7, 12, 13]. MEDA is based on the concept of a sea-of-micro-electrodes with an array of identical basic microfluidic unit components called microelectrode cells (MCs) [12], as illustrated in Figure 1. Each MC consists of a microelectrode and a control/sensing circuit. MEDA allows microelectrodes to be dynamically grouped under program control to form a micro-component (e.g., mixer or diluter) that can perform different microfluidic operations on the chip. Prototypes of MEDA-based biochips have been fabricated using TSMC 0.35 μm CMOS technology.

A major obstacle that impedes reliable microfluidic operations on MEDA biochips is the lack of adaptive and efficient techniques that can facilitate recovery from unexpected errors. Faults in MEDA biochips may arise during bioassay execution. For example, excessive actuation voltage may lead to electrode breakdown and charge trapping [5], and DNA fouling may lead to the malfunction of multiple electrodes in the biochip [21]. Such faults may eventually result in errors (e.g., a splitting operation with unbalanced droplets), which can adversely impact the correctness of fluidic operations.

In order to ensure robust fluidic operations and high confidence in the outcome of biochemical experiments, error-recovery techniques have recently been proposed [8, 11, 17, 24]. Zhao et al. [24] proposed an efficient control-path design method based on error-propagation estimates for fluidic operations. Luo et al. [17] presented a cyberphysical approach that uses sensor data at intermediate checkpoints to dynamically reconfigure the biochip. Jaress et al. [11] proposed a roll-back-based error-recovery technique that leverages a virtual topology to quickly obtain resynthesis results.

All the above techniques are targeted at conventional DMFBs, therefore they can not fully exploit the advantages specific to MEDA-based biochips (e.g., real-time droplet sensing). For MEDA biochips, Li et al. [15] recently presented an error-recovery strategy based on local adaptation (i.e., "local recovery"), and analyzed it using probabilistic timed automata (PTA). A control flow was also proposed to connect local recoveries with global recovery. However, despite its benefits, this method has several shortcomings:

- It uses static error-recovery protocols for local errors, i.e., the error-recovery protocols are identical for the same type of errors irrespective of when or where on the chip they occur. This approach is not efficient for minimizing the recovery overhead, e.g., sample cost and chip-area impact.
- The solution in [15] makes an unrealistic assumption that resources are always available for local recovery, e.g., there is always a sufficient number of fluidic modules for re-execution of operations. In practice, however, the available resources must be considered in making decisions about local recovery.
- In [15], the same recovery time is assigned for each operation, which is not efficient in minimizing the time spent on error recovery. The recovery-time assignment must consider various factors, e.g., the type and the extent of detected errors, to determine the recovery time for each detected local error.
- Finally, [15] uses all the assigned recovery time for local errors, and it does not consider the likelihood that the local recovery can be successfully completed using less recovery time. Thus, a more adaptive synthesis technique is needed to derive online synthesis results to guide execution of the remaining microfluidic operations.

To overcome the above drawbacks, this paper advances error-recovery by exploring (i) a flexible error-recovery solution derived using formal methods, and (ii) adaptive online synthesis based on real-time sensing results. The proposed approach provides error tolerance with significantly reduced recovery cost and higher probability of success. The main contributions of this paper are:

- We model the error-recovery procedure using Markov decision processes (MDPs). We also describe the platform as another MDP, composing a unified model using stochastic multi-player games.
- We formalize the error-recovery objectives and use them to synthesize optimal error-recovery protocols for local recovery. The system behaviors under the optimal protocols are then analyzed.
- We describe an efficient method to determine available recovery resources for each detected error. Based on the available resources, we dynamically assign the recovery time for different local errors.
- We present an adaptive online synthesis flow to recompute new schedules, module placements, and droplet routes on-the-fly in response to errors.

The rest of the paper is organized as follows. Section 2 presents an overview of MEDA biochips and formal methods that are relevant to this work. In Section 3, we present the problem formulation before describing the synthesis of error-recovery protocols for local errors in Section 4. Section 5 presents an adaptive online synthesis technique for global error recovery. Experimental results on real-life benchmarks, as well as comparison with [15], are presented in Section 6. Finally, Section 7 concludes the paper.

2 PRELIMINARIES

In this section, we provide an overview of digital microfluidics and MEDA, as well as experimental results that illustrate the need for probabilistic modeling of MEDA operations. We then provide an introduction to the formal methods used for modeling, design and analysis of stochastic systems, which are utilized for the synthesis of optimal error-recovery protocols in Section 4.

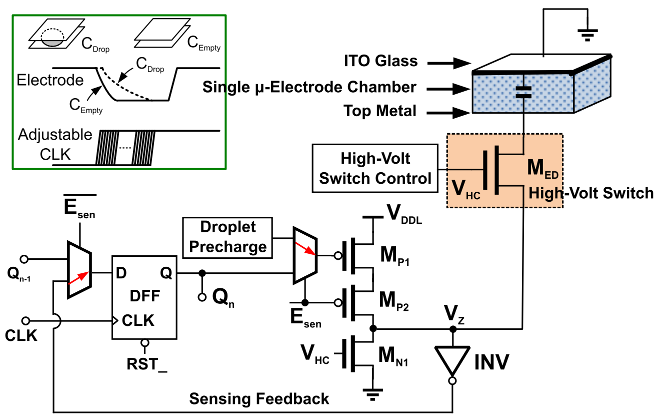

Fig. 2. Sensing circuit in MEDA biochips [7].

2.1 Digital Microfluidics and MEDA

A DMFB is able to manipulate and move picoliter droplets containing biological samples on a two-dimensional electrode array. MEDA extends this basic architecture by adding more flexibility [12]. Furthermore, the size of the microelectrodes can be 10 times smaller (e.g., 100 μm in length) than conventional electrodes. The MEDA biochip consists of microelectrode cells (MCs). Each MC includes a microelectrode, an activation circuit, and a sensing circuit [13].

2.1.1 Sensing Scheme in MEDA. In contrast to conventional DMFBs, real-time sensing can be achieved on MEDA biochips. MEDA biochips can detect the property (droplet-property sensing) and the location (droplet-location sensing) of on-chip droplets. Sensing results are presented in the form of a sensing map. Figure 2 shows the diagram of the sensing circuit in a MEDA biochip. The parasitic capacitance with and without droplets between the top reference electrode and the bottom microelectrode is defined as C_{Drop} and C_{Empty}, respectively. During droplet-location sensing, droplet precharge circuit first charges the parasitic capacitor. Transistor M_{N1} is then turned on to discharge the parasitic capacitor. Due to the difference between capacitances C_{Drop} and C_{Empty}, INV outputs different voltage levels. Similar to droplet-location sensing, droplet-property sensing utilizes the capacitance difference between different types of droplets to generate different charging and discharging time.

Sensing on MEDA biochips can provide users with detailed information about the outcomes of on-chip operations. Therefore, errors can be detected in real-time, and error-recovery techniques can then be invoked for error correction.

2.1.2 Outcome Classification. As described in [15], the outcomes of fluidic operations can be experimentally classified into three categories: *minor error*, *major error*, and *no error*. The classification is based on the level of completeness (LOC) of an operation. The LOC measures the extent to which an operation is complete within a pre-specified window, compared with the ideal case (e.g., a uniform mixing and a balanced splitting), and it ranges between 0 and 1—a larger LOC represents a higher degree of completeness. Here, we use formulas from [15] to calculate the LOC for every operation.

To obtain outcome probabilities for mixing and splitting operations, we performed 100 mixing and 100 splitting operations on a MEDA biochip. The corresponding LOC for each operation was obtained and the distribution of LOCs for mixing and splitting operations are shown in Figure 3.

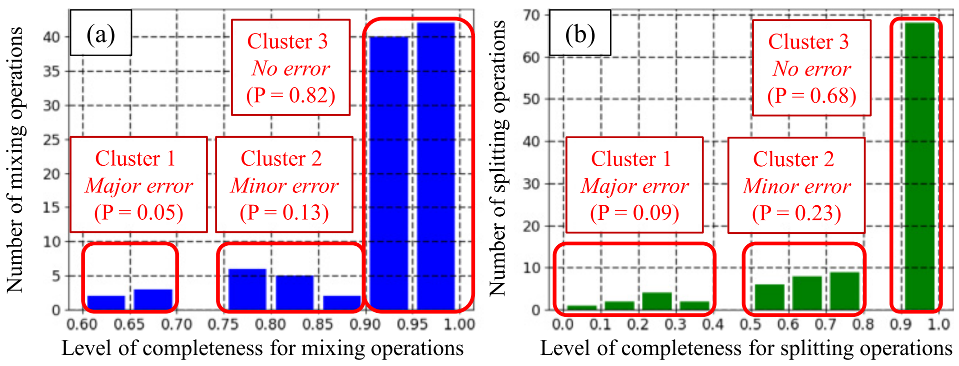

Fig. 3. Experimental results for LOC distributions; P is the outcome probability for a $\langle$*operation*, *category*$\rangle$ pair.

Based on Figure 3, the probabilities that the outcome of a mixing operation is a major error, minor error, and no error are 0.05, 0.13, and 0.82, respectively. Also, the probabilities that the outcome of a splitting operation is a major error, minor error, and no error are 0.09, 0.23, and 0.68, respectively.

2.2 Formal Modeling of Stochastic Processes

2.2.1 Markov Decision Processes (MDPs). MDPs are a formalism widely used to model systems that exhibit both stochastic and nondeterministic behaviors. MDPs are similar to Finite-State Machines, with standard guards, specifying the logical conditions that enable transitions [1], and nondeterministic actions/events that can be used in addition to probabilistic transitions. Stochastic behaviors capture scenarios when a system randomly, with predefined probability distributions, evolves from one state to another [19]. In contrast, nondeterministic behavior means that the system can evolve to the next state via any enabled transition, in a way that is unknown. Intuitively, nondeterminism captures choices that a system (e.g., controller or environment) could make; in every state, once a nondeterministic choice is made, the next state is selected in a probabilistic manner, as in Discrete-Time Markov Chains (DTMC).

Formally, an MDP is specified as a tuple $\mathcal{M} = \langle \mathcal{S}, \mathcal{A}, \delta, s_0 \rangle$, where: (a) S is a finite set of states and $s_0 \in \mathcal{S}$ is the initial state; (b) $\mathcal{A}$ is a finite set of actions; and (c) $\delta : \mathcal{S} \times \mathcal{A} \times \mathcal{S} \rightarrow [0,1]$ is a transition probability function such that for all $s \in S$ and $\alpha \in \mathcal{A}$, it holds $\sum_{s' \in \mathcal{S}} \delta(s, \alpha, s') \in \{0, 1\}$. Note that if action α is enabled in s, no matter if it is active or inactive, the sum should be equal to 1; otherwise, it is equal to 0. We use $\mathcal{A}(s) \subseteq \mathcal{A}$ to denote the set of enabled actions in s. For any state $s \in \mathcal{S}$, it is required that $\mathcal{A}(s) \neq \emptyset$. When there is more than one action available in state s (i.e., $|\mathcal{A}(s)| > 1$), a nondeterministic choice should be made; on the other hand, if for all s it holds that $|\mathcal{A}(s)| \leq 1$, then the MDP is effectively a DTMC. The system evolution starts in s_0. At each step, the system moves from s to s' with probability $\delta(s, \alpha, s')$ if there exists a transition $s \xrightarrow{g:\alpha} s'$ such that the guard g holds and action a is active. Note that this transition is probabilistic if $\delta(s, \alpha, s') \in (0, 1)$ or deterministic if $\delta(s, \alpha, s') = 1$.

2.2.2 Model Composition. When modeling complex systems, it is more favorable to use a number of MDPs to capture the behavior of different system components instead of adopting a monolithic approach. Model composition can then be used to merge those models after defining the synchronization rules among them. Let $\mathcal{M}_1 = \langle S_1, \mathcal{A}_1, \delta_1, s_1 \rangle$ and $\mathcal{M}_2 = \langle S_2, \mathcal{A}_2, \delta_2, s_2 \rangle$ be two MDPs. The parallel composition of the MDPs is defined as

$$\mathcal{M}_1 \parallel \mathcal{M}_2 = \langle S_1 \times S_2, \mathcal{A}_1 \times \mathcal{A}_2, \delta, (s_1, s_2) \rangle.$$

Intuitively, MDPs are composed by synchronizing on common actions (the probability function is then the product of distributions for δ_1 and δ_2) and interleaving otherwise. In the former case, MDPs can synchronize over *channels*. Here, a transmitter over a channel α (denoted by $\alpha!$) must synchronously execute with all receivers (denoted by $\alpha?$) only if all guards associated with α are satisfied. More about MDP semantics and composition can be found in [19].

2.2.3 Stochastic Multi-Player Games (SMGs). SMGs are similar to MDPs, where nondeterministic choices are resolved by more than one entity, called players. SMGs facilitate modeling systems with more than one source of nondeterminism. Formally, an SMG is defined as a tuple $\mathcal{G} = \langle \Upsilon, S, \mathcal{A}, \delta, s_0 \rangle$, where: (a) Υ is a finite set of players; (b) S is a finite set of states, partitioned into disjoint set of states $S_v,\ v \in \Upsilon$; (c) $\mathcal{A}$ is a finite set of actions; (d) $\delta : S \times \mathcal{A} \times S \rightarrow [0,1]$ is a partial transition function; and (e) $s_0 \in S$ is the initial state. A state $s \in S_v$ is controlled by player v, i.e., the nondeterministic choices from s are controlled by v. If $s \in S_0$, then the next state is chosen probabilistically. More details on SMGs can be found in [3].

2.2.4 Specifications. We use temporal logic to formally specify model properties that we would like to analyze. Specifically, to express properties for SMGs we use rPATL—Probabilistic Alternating-time Temporal logic with Rewards [3]. For instance, consider a game $\mathcal{G}$ where v is a player and φ is a predicate that is satisfied in some state s (i.e., $s \models \varphi$). Consider the rPATL formulas

$$\phi_1 \coloneqq \langle\langle v \rangle\rangle \delta_{\geq q} \left[\Diamond \varphi \right], \quad \phi_2 \coloneqq \langle\langle v \rangle\rangle \mathcal{R}^r_{\geq x} \left[\Diamond \varphi \right].$$

Formula ϕ_1 asks if v can eventually reach a state s satisfying property φ (i.e., $s \models \varphi$) with probability that is greater than or equal to q, while ϕ_2 checks if the accumulated rewards (associated with transitions and states) before reaching a state s satisfying φ (i.e., $s \models \varphi$) is greater than or equal to x. Alternatively, the quantitative queries

$$\langle\langle v \rangle\rangle \delta_{max=?} \left[\Diamond \varphi \right], \quad \langle\langle v \rangle\rangle \mathcal{R}^r_{max=?} \left[\Diamond \varphi \right]$$

seek the maximal numerical values rather than assertions. More about specification semantics and rPATL can be found in [3].

2.2.5 Strategies and Synthesis Problem. Given an SMG $\mathcal{G}$, a strategy π is a set of rules to resolve all nondeterministic choices of a player v, reducing the model into an MDP $\mathcal{M}^\pi$. The synthesis problem is an attempt to answer the following question: *Given an SMG $\mathcal{G}$ and a specification ϕ, find a strategy π for player v such that for all opponents strategies σ, the induced DTMC satisfies the specification*—i.e., $\mathcal{G}^{\pi,\sigma} \models \phi$ for all possible opponent strategies σ. More about strategy synthesis can be found in [22].

3 PROBLEM FORMULATION

To map a bioassay to a MEDA biochip, synthesis techniques [14] are required to bind the assay operation to on-chip resources and generate an optimized schedule of fluidic operations. The input bioassay is modeled by a sequencing graph [10], which denotes the dependencies between fluidic operations. As discussed in Section 1, errors may occur during the execution of bioassays on a MEDA biochip. A MEDA biochip is said to have an error if its operation does not match its specified behavior. In this work, we assume that chips have been carefully tested before they can be used for bioassay execution, i.e., we assume that droplets will never be stuck during their transportation and droplet dispensing can always be successfully achieved. However, some manufacturing defects may be latent, and they may produce errors during field operation [15]. Thus, we focus on developing error-recovery approaches for online errors, i.e., mixing and splitting errors during bioassay execution.

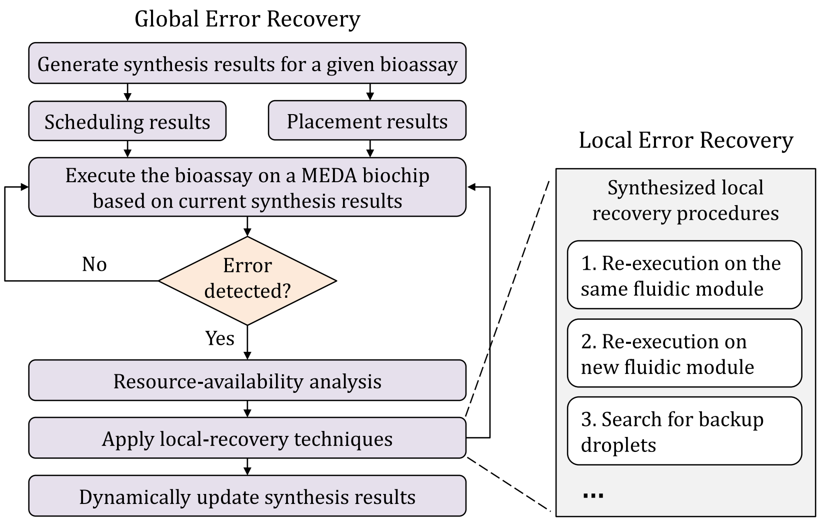
Global Error Recovery
Generate synthesis results for a given bioassay
Scheduling results
Placement results
Execute the bioassay on a MEDA biochip based on current synthesis results
Error detected?
No
Yes
Resource-availability analysis
Apply local-recovery techniques
Dynamically update synthesis results
Local Error Recovery
Synthesized local recovery procedures
1. Re-execution on the same fluidic module
2. Re-execution on new fluidic module
3. Search for backup droplets
...

Fig. 4. Relationship between local and global error recovery.

For a given bioassay, we use on-chip sensing to evaluate the quality of output droplets of each mixing and splitting operation. Recall that MEDA can provide real-time sensing results for on-chip operations, and thus the time required for outcome evaluation is negligible. Once an error is detected, a local recovery approach is desired to recover from the error. *Local recovery* for a specific error refers to adaptation actions that are invoked to maximize probability of success for the operation that was affected by that error. However, local error recovery requires extra chip area and consumes time, which may result in a conflict with the original schedule [11]. Consequently, we also focus on *global error recovery* to efficiently coordinate local-recovery procedures for the complete bioassay. The focus of global recovery is on (i) dynamic assignment of resources used for local recoveries, and (ii) generating new synthesis results (i.e., operation scheduling and module placement) to reduce the interference between error-recovery procedures and bioassay execution. The relationship between local and global error recovery is shown in Figure 4. The formal models reviewed in Section 2, and described in more detail in Section 4, allow us to make informed decisions about the local recovery procedures, and hence they also play a role in efficient global recovery.

The objective of this work is to develop an error-recovery strategy that can minimize the impact on bioassay completion time and maximize the probability of successful error recovery. The strategy includes approaches for both local recovery (for erroneous operations) and global recovery (for the complete bioassay). For local recovery, we introduce an optimal recovery approach that maximizes the probability of successful recovery based on available resources. For global recovery, we introduce an online synthesizer to seamlessly connect local recovery with global recovery.

3.1 Strategy Overview

The proposed error-recovery strategy (Figure 5) contains two major components: (i) online synthesizer, which is used to dynamically adjust operation scheduling and module placement, and (ii) local error recovery model that, based on available resources, provides an optimal local-recovery protocol. These components seamlessly coordinates with each other for the implementation of the proposed error-recovery strategy on the hardware platform.

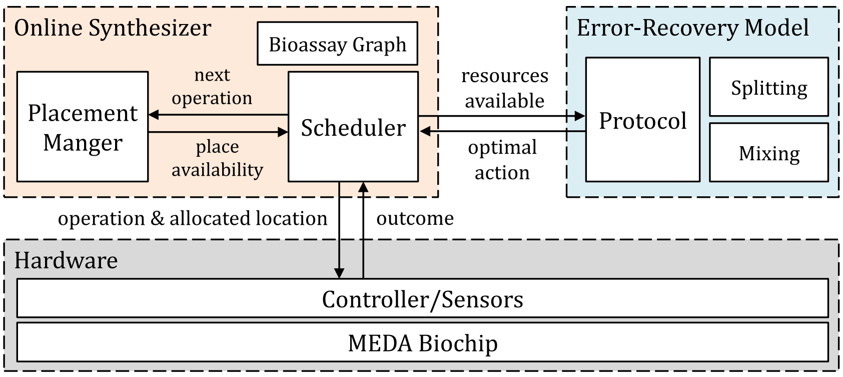

Fig. 5. Overview of the proposed error-recovery strategy.

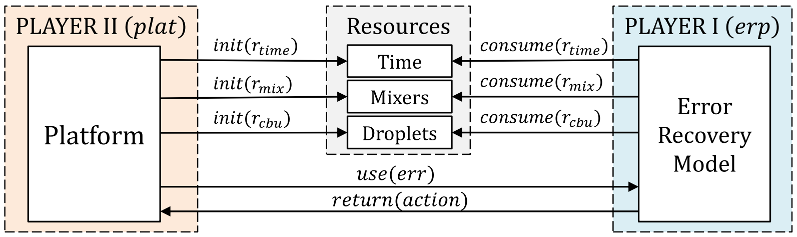

Fig. 6. Data flow structure of the error-recovery model.

Details of the error-recovery model and online synthesizer are presented in Section 4 and Section 5, respectively. The error-recovery model is used *offline* to generate optimal error-recovery protocols for any level of available resources. Then, all these optimal error-recovery protocols are stored in a lookup table. At *runtime*, if an error is detected during the execution of a bioassay, the *online* synthesizer first performs an analysis on available resources and then obtains the optimal recovery protocol from the constructed lookup table. Finally, the online synthesizer dynamically adjusts synthesis results to avoid interference between error-recovery protocols and the execution of following operations.

4 MODELING AND SYNTHESIS OF LOCAL ERROR-RECOVERY PROTOCOLS

In this section, we introduce a method to design optimal error recovery protocols for any level of available system resources (e.g., time for recovery, mixers). We start by constructing MDP models of the error recovery process for various fluidic operations. These models, along with an abstracted model of the platform, are obtained from the experimental data presented in Section 2.1, and then integrated using model composition to obtain an SMG model of the system. Finally, we formalize the error-recovery process objectives and use them to *automatically* synthesize optimal error-recovery protocols.

4.1 Error-Recovery Model

Consider a bioassay that includes a combination of mixing, splitting and dilution operations. Figure 6 shows the data flow structure of the error-recovery process, which forms the basis of our formal model. The model captures the control execution as well as the probabilistic behavior of the platform. When a bioassay operation is performed, the resource manager updates the amount of resources that can be allocated for error recovery (i.e., available time r_{time}, mixers r_{mix}, and

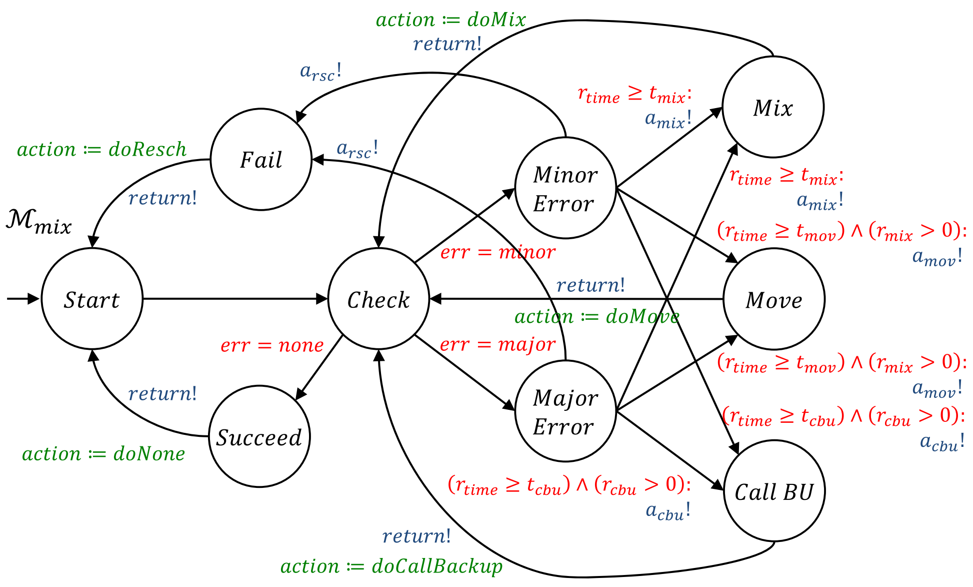
$\mathcal{M}_{mix}$
Start
Check
Fail
Succeed
Minor Error
Major Error
Mix
Move
Call BU
$action \coloneqq doMix$
$return!$
$a_{rsc}!$
$a_{rsc}!$
$action \coloneqq doResch$
$return!$
$r_{time} \geq t_{mix}$: $a_{mix}!$
$r_{time} \geq t_{mix}$: $a_{mix}!$
$(r_{time} \geq t_{mov}) \wedge (r_{mix} > 0)$: $a_{mov}!$
$err = minor$
$return!$
$action \coloneqq doMove$
$err = none$
$err = major$
$(r_{time} \geq t_{mov}) \wedge (r_{mix} > 0)$: $a_{mov}!$
$(r_{time} \geq t_{cbu}) \wedge (r_{cbu} > 0)$: $a_{cbu}!$
$return!$
$action \coloneqq doNone$
$(r_{time} \geq t_{cbu}) \wedge (r_{cbu} > 0)$: $a_{cbu}!$
$return!$
$action \coloneqq doCallBackup$

Fig. 7. Error-recovery model for mixing ($\mathcal{M}_{mix}$).

backup droplets r_{cbu}), while the platform provides the information about the operation outcome. Based on this information, the error-recovery model identifies both optimal actions and resources required to recover from the error.

4.1.1 Mixing Error-Recovery Model ($\mathcal{M}_{mix}$). We start by considering the error-recovery model $\mathcal{M}_{mix}$ for mixing operations (Figure 7). Initially, the model moves to *Check* state, where the process outcome is checked. This outcome falls into one of three categories as shown in Figure 3, namely successful, unsuccessful with minor error or with major error, upon which the model moves to the corresponding state. For successful outcome, the model returns to *Start*, signaling the action *doNothing*. Otherwise, in *Minor Error* or *Major Error* states, four actions are available to choose from.

The first three actions are to reuse both the same droplet and mixer (a_{mix}), to move the droplet to a new mixer (a_{mov}), and to use a backup droplet to complete the operation (a_{cbu}). Each of these actions is guarded by the availability of the required resources, and further ensures that such resources are consumed by synchronizing with the resources model (described in Section 4.1.4). Depending on the selected action, the model progresses to *Mix*, *Move* or *Call BU* state, before returning to *Check* by accordingly updating the variable *action*. The fourth action a_{rsc} captures rescheduling of the mixing operation, when the process aborts by moving from *Fail* to *Start*.

4.1.2 Splitting Error-Recovery Model ($\mathcal{M}_{split}$). Similar to the mixing operation, an error-recovery protocol for a splitting operation starts by reading its outcome. The process aborts by moving from *Check* to *Start* states if the operation is successful. Otherwise, it moves to either *Minor Error* or *Major Error* states, from which it can proceed with a_{merge}, $a_{reroute}$ or a_{rsc} actions to *Merge*, *Reroute* or *Schedule* states, respectively. While actions a_{merge} and $a_{reroute}$ request merging the defective droplets or rerouting to a new splitter before any further splitting attempts, the action a_{rsc} requests rescheduling. The variable *action* is used to store the decision made upon synchronizing over *return* action.

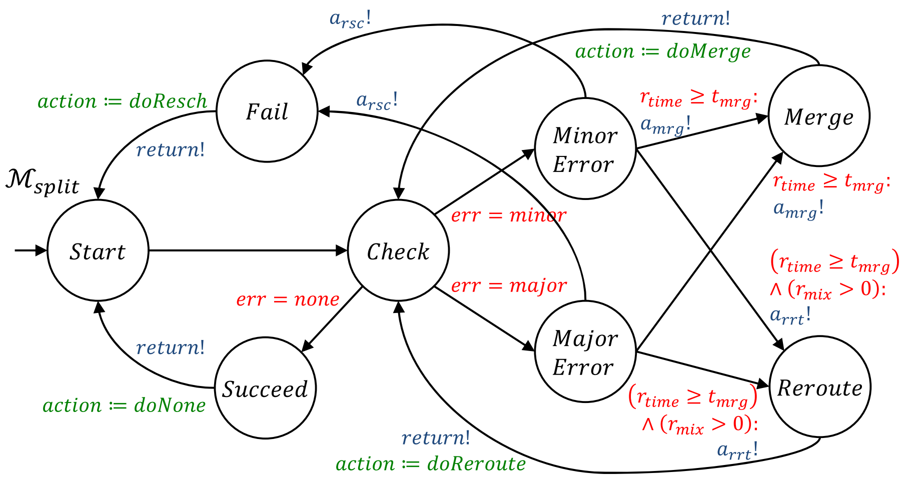

Fig. 8. Error-recovery model for splitting ($\mathcal{M}_{split}$).

Table 1. List of Corrective Actions and Associated Costs

		Resources Consumed		
Operation	Action	Time	Locations	Droplets
Mixing	Retry Mixing	2s	0	0
	Move Droplet	2s	1	0
	Call Backup	2s	0	1
	Reschedule	0s	0	0
Splitting	Merge	1s	0	0
	Move Droplet	1s	1	0
	Reschedule	0s	0	0

4.1.3 Dilution Error-Recovery Model. In a dilution operation, a droplet first undergoes a mixing operation, after which it is split into two droplets. Hence, we construct the dilution error-recovery model $\mathcal{M}_{dilute}$ as $\mathcal{M}_{mix}$ followed by $\mathcal{M}_{split}$.

4.1.4 Resources Model. Each error-recovery action is associated with specific resource demands, as shown in Table 1. We model these resources as DTMCs from Figure 9 with: $\mathcal{M}_{time}$ tracking time through r_{time} variable, $\mathcal{M}_{mixers}$ tracking the number of mixers r_{mix}, $\mathcal{M}_{drop}$ tracking the number of backup droplets r_{cbu}, $\mathcal{M}_{actMix}$ tracking current mixer condition through *mixer* variable, and $\mathcal{M}_{actDrp}$ tracking current droplet condition *droplet*. All five variables are initialized by receiving *init* action, triggered by $\mathcal{M}_{plat}$ (Figure 10). These variables are also updated by one or more of the actions a_{mix}, a_{mov}, a_{cbu}, a_{mrg}, and a_{rrt}, triggered by $\mathcal{M}_{mix}$ (as in Figure 7) or $\mathcal{M}_{split}$ (Figure 8). The action *use*, triggered by $\mathcal{M}_{plat}$ (Figure 10, described in Section 4.1.5), marks the current droplet and mixer as used by assigning the value *isOld* to both *droplet* and *mixer* variables, while actions a_{mov} and a_{cbu} set the variables back to *isNew*.

4.1.5 Platform Model ($\mathcal{M}_{plat}$). Since our focus is on the local error-recovery process, it is imperative that the system model captures two fundamental aspects—operation outcome and resources availability. In a typical MEDA biochip, on-chip sensors provide real-time measurements of a process outcome. Being unknown at design stage, we assume that the outcome follows a

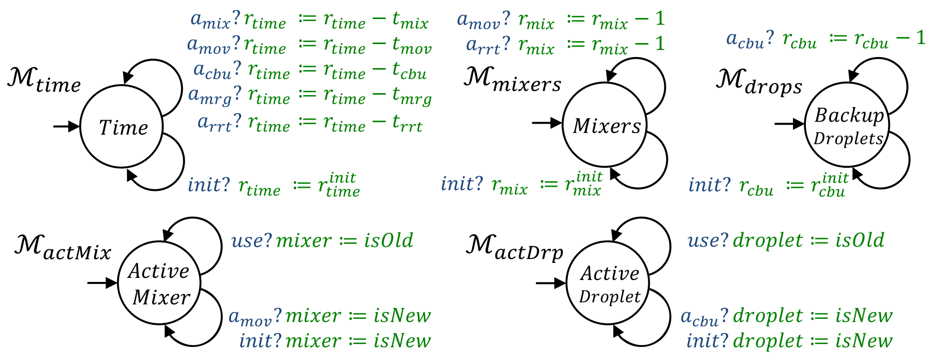

$\mathcal{M}_{time}$
Time
$a_{mix}?\, r_{time} := r_{time} - t_{mix}$
$a_{mov}?\, r_{time} := r_{time} - t_{mov}$
$a_{cbu}?\, r_{time} := r_{time} - t_{cbu}$
$a_{mrg}?\, r_{time} := r_{time} - t_{mrg}$
$a_{rrt}?\, r_{time} := r_{time} - t_{rrt}$
$init?\, r_{time} := r_{time}^{init}$
$\mathcal{M}_{mixers}$
Mixers
$a_{mov}?\, r_{mix} := r_{mix} - 1$
$a_{rrt}?\, r_{mix} := r_{mix} - 1$
$init?\, r_{mix} := r_{mix}^{init}$
$\mathcal{M}_{drops}$
Backup Droplets
$a_{cbu}?\, r_{cbu} := r_{cbu} - 1$
$init?\, r_{cbu} := r_{cbu}^{init}$
$\mathcal{M}_{actMix}$
Active Mixer
$use?\, mixer := isOld$
$a_{mov}?\, mixer := isNew$
$init?\, mixer := isNew$
$\mathcal{M}_{actDrp}$
Active Droplet
$use?\, droplet := isOld$
$a_{cbu}?\, droplet := isNew$
$init?\, droplet := isNew$

Fig. 9. Model of resources.

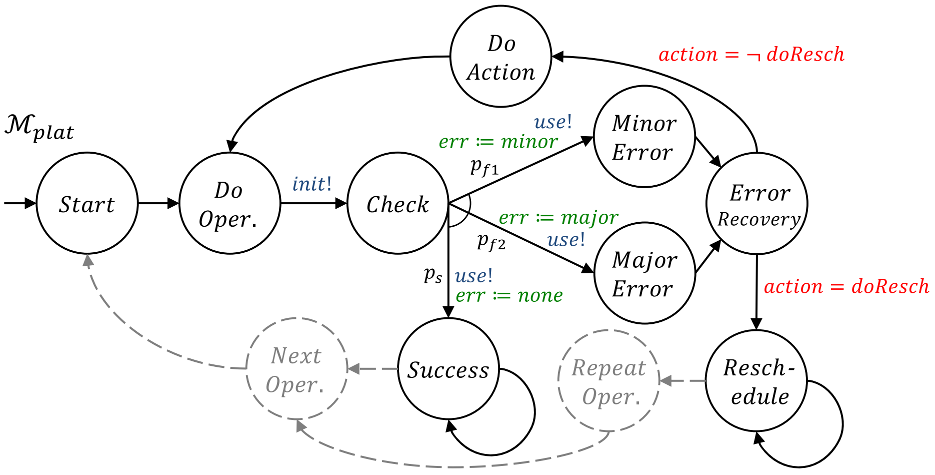

Fig. 10. Platform abstraction model ($\mathcal{M}_{plat}$).

uniform probability distribution, an assumption supported by the experimental results presented in Section 2.1. Nevertheless, one limitation of the aforementioned results is that they only characterize the outcome probability of an operation at its first attempt. Hence, in Table 2 we augment these results with a model of how the error type of last trial and droplet and mixer conditions may influence the outcome probability of a recovery operation, mostly due to mixer degradation as discussed in [9, 18]. We assume that the probability of the outcome to be successful is the highest when the droplet and mixer used are both new. Similar model is used for splitting operations.

Figure 10 shows the MDP $\mathcal{M}_{plat}$ that captures the probabilistic behavior of the platform by abstracting the scheduler, controller, sensors and biochip. The model moves from *Start* to *Do Operation* state when an operation is being processed. The transition from *Do Operation* to *Check* is associated with the *init* action, which synchronizes with the resources model (from Figure 9) to initialize the available resources. The transition exiting *Check* state is sampled from a uniform distribution characterized by p_s, p_{f1} and p_{f2}. These probabilities, rather than being constant, depend on the variables *droplet*, *mixer*, and *err* (from Table 2), where *err* denotes the last type of error. Any of these three probabilistic transitions triggers the action *use*, marking both the droplet and mixer as used, and assigns a new value to *err*.

Table 2. Probability Distributions Over the Possible Outcomes of Mixing and Splitting Process.

Resource		Previous	Mixing Outcome			Splitting Outcome		
Droplet	Mixer	Outcome	p_s	p_{f1}	p_{f2}	p_s	p_{f1}	p_{f2}
New	New	N/A	0.820	0.130	0.050	0.680	0.230	0.090
New	Used	minor error	0.656	0.248	0.096	0.408	0.426	0.166
New	Used	major error	0.164	0.232	0.604	0.204	0.224	0.572
Used	New	minor error	0.492	0.367	0.141	0.544	0.328	0.128
Used	New	major error	0.246	0.209	0.545	0.136	0.243	0.621
Used	Used	minor error	0.328	0.485	0.187	0.272	0.523	0.205
Used	Used	major error	0.082	0.255	0.663	0.068	0.262	0.670

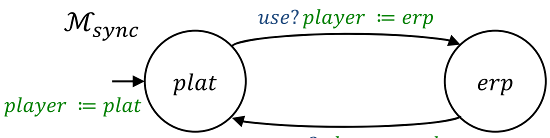

Fig. 11. Synchronization model ($\mathcal{M}_{sync}$).

If the sampled outcome leads to either *Minor Error* or *Major Error*, the model proceeds to *Error Recovery*. The next state is defined according to the action defined by $\mathcal{M}_{mix}$ or $\mathcal{M}_{split}$ through the variable *action*. Any action other than rescheduling leads to *Do Action* state and subsequently back to *Do Operation* state, where the operation is repeated after the corrective action is done. In contrast, if $action = doResch$, the model moves to *Reschedule* state, which marks unsuccessful attempt to recover from the error. On the other hand, if the sampled outcome leads to *Success*, the operation ends. While $\mathcal{M}_{plat}$ in Figure 10 models a single bioassay operation, for a sequence of operations the model can be augmented with the grayed extension (Figure 10) to execute in a loop parsing a list of operations.

4.2 Model Composition

The aforementioned models present the components and functionalities of a MEDA-based system. The overall system model is obtained by composing those models along with a synchronization model $\mathcal{M}_{sync}$ from Figure 11, to ensure a turn-based synchronization—i.e., that only one action is triggered at a time. This is achieved using the variable *player* that indicates which model is allowed to execute actions. In addition, all transitions of models capturing error-recovery process (i.e., $\mathcal{M}_{mix}$ and $\mathcal{M}_{split}$) are guarded by $player = erp$, while all transitions of the platform model $\mathcal{M}_{plat}$ are guarded by $player = plat$. All other models, capturing available resources, are reactive as they do not trigger any actions, and thus none of the player-based global guards are needed.

As the error-recovery protocol is triggered after a platform error occurs, $\mathcal{M}_{sync}$ is initialized with $player = plat$, i.e., $\mathcal{M}_{plat}$ progresses first. Whenever the platform model decides on the operation (i.e., *init* is triggered—see Figure 10), $\mathcal{M}_{plat}$ is halted (i.e., $player = erp$). Then, depending on the selected operation, either $\mathcal{M}_{mix}$ or $\mathcal{M}_{split}$ becomes active. Similarly, when an operation either succeeds or fails (i.e., *return* is triggered—see Figure 7 and Figure 8), the control goes back to the platform model $\mathcal{M}_{plat}$.

The overall system model can be established through parallel composition. If initial values for the resources are assumed to be fixed then only one source of nondeterminism exists, and hence the system model is an MDP. However, synthesized protocols based on this assumption are only optimal for that specific number of available resources. We relax this assumption by allowing $\mathcal{M}_{plat}$ to nondeterministically select the initial (i.e., available) resources. Thus, the overall system model is an SMG, denoted by $\mathcal{G}_{sys}$, and defined as

$$\begin{aligned}\mathcal{G}_{sys} = \mathcal{M}_{plat} \parallel \mathcal{M}_{mix} \parallel \mathcal{M}_{split} \parallel \mathcal{M}_{time} \parallel \mathcal{M}_{mixers}\\ \parallel \mathcal{M}_{drop} \parallel \mathcal{M}_{actMix} \parallel \mathcal{M}_{actDrp} \parallel \mathcal{M}_{sync}.\end{aligned}$$

Finally, the game is played between the error-recovery process, denoted by *erp*, and the platform, denoted by *plat*.

4.3 Strategy Synthesis

In order to synthesize optimal strategies for error recovery, we use the composed SMG model $\mathcal{G}_{sys}$ to find an error-recovery policy that satisfies a specification capturing the desired optimality objective. We define the objective (i.e., specification) of the optimal protocol as follows: *Given a set of resources, find the recovery action that maximizes the probability that the process is eventually successful.* This objective can be formally expressed with the rPATL query [3]

$$\phi \coloneqq \langle\langle erp \rangle\rangle\, \mathcal{P}_{max=?}\ [\ \varphi \coloneqq \Diamond\ Succeed\ ],$$

where $\Diamond$ is the temporal operator *eventually*. Hence, the synthesis problem aims to find the optimal strategy π^* such that

$$\mathcal{G}_{sys}^{\pi^*,\sigma} \models \phi \qquad \forall \sigma \in \Sigma,$$

where Σ is the set of all possible opponent (i.e., platform) strategies. Although the query ϕ results in a single value for $\mathcal{P}_{max}$, the synthesis problem seeks the strategy that maximizes the probability $\mathcal{P}$ for every possible opponent strategy $\sigma \in \Sigma$, i.e., for every possible assigned resources, resulting in an optimal error-recovery protocol.

We use PRISM-games [4] to implement $\mathcal{G}_{sys}$ along with the query ϕ. The maximum probability of satisfying φ at state s can be found using *value iteration* algorithm [3], which is implemented in PRISM-games. For the obtained optimal recovery policies, in Section 6.1 we investigate the relationship between several attributes, such as the effect of resource availability on the probability of success for these operations.

5 GLOBAL ERROR RECOVERY

The local error-recovery protocols, derived offline using the techniques from Section 4, depend on the upper limit on the recovery time and the set of available resources that can be used for recovery. However, to adaptively invoke error recovery for the bioassay, we need a global error-recovery technique that can tackle two key problems. First, to determine an optimal error-recovery policy, the local error recovery model must have knowledge of the available resources, e.g., the number of fluidic modules and backup droplets, as well as the time available for recovery. Second, multiple errors can occur at different locations on the chip at nearly the same time, and the error-recovery procedures for these errors can be intertwined through resource sharing or droplet-path overlap. Therefore, there is a need to dynamically generate new schedules and module placements for error recovery and other bio-protocol-related operations, such that the adverse impact of error-recovery procedures on protocol execution is minimized. In this section, we first describe how we determine resource availability. Next, an online synthesis approach is presented to dynamically generate new schedules and module placements in response to local-recovery decisions.

5.1 Inputs to Local Error Recovery

Recall that the local error recovery requires information about the number of backup droplets, the number of fluidic modules available, and the maximum allowable recovery time. We next describe how these parameters are determined.

5.1.1 Available Backup Droplets. For a splitting or a dilution operation, if only one of its output droplets is used as an input for an immediate successor, the other (redundant) droplet is referred to as a *backup droplet* for possible error recovery. In addition, dispensing operations can be scheduled for execution as early as possible and extra droplets can be stored on the biochip as backup. Unused backup droplets are sent to the waste reservoir upon the completion of the bioassay.

The number of backup droplets available for an operation can be determined from the sequencing graph. In a sequencing graph, each node represents an operation. Let $BU(O_i)$ denote the number of backup droplets generated by operation O_i. Suppose operation O_j is an immediate successor of the N operations denoted by $O_{j_1}, O_{j_2}, \ldots O_{j_N}$. Then, the number of available backup droplets for the operation O_j is $\min(BU(O_{j_1}), BU(O_{j_2}), \ldots, BU(O_{j_N}))$, since operation O_j requires one droplet from each of its immediate predecessors.

5.1.2 Available Fluidic Modules. A fluidic module is a group of microelectrodes on a MEDA biochip that can be configured to perform a type of operation (e.g., mixing). In order to determine the number of fluidic modules available for local error recovery, we use a search algorithm based on the notion of a forbidden set introduced in [16]. A *forbidden set* refers to a set of locations where new fluidic modules cannot be placed.

If an error occurs for an operation, the algorithm attempts to place appropriate fluidic modules on the biochip so that they can be used for local error recovery. The forbidden set is used to avoid placement conflicts with other operations. This algorithm terminates when either (1) a total of N fluidic modules are placed on the biochip, where N refers to the maximum number of fluidic modules designated for use in local error recovery (determined by the local error-recovery model), or (2) not enough space is available to place a fluidic module. When this algorithm terminates, it provides the number and the locations of fluidic modules for local error recovery.

The pseudo-code for determining the number of fluidic modules is shown in Figure 12. The parameter *fluidic_modules* is a container, which stores the placements of available fluidic modules (line 1). According to the current module placement MP, we use the function *getPlacementSet*() to obtain the set of available locations PS for a fluidic module (line 2). If PS is not empty, i.e., there is sufficient space to place a new fluidic module, the function *findBestPlacement*() is used to find the module placement MP_{new} with minimum cost (lines 3–4). The cost is defined as the Manhattan distance [16] between the target fluidic module and the erroneous fluidic module. The newly identified fluidic-module placement is stored in *fluidic_modules* (line 5). Next, we examine the number of fluidic-module placements in the container: (1) if we already have N fluidic-module placements, the search is stopped; (2) otherwise, the newly found fluidic-module placement MP_{new} is added to the on-chip module placement set MP, and we continue the search for another fluidic-module placement based on the updated MP (lines 6–9). Finally, when the search stops, we delete the newly added fluidic module placements from MP (lines 12–14) and get the number and the locations of fluidic modules from *fluidic_modules* (line 15). For a MEDA biochip with an $M \times N$ microelectrode array, the computational complexity of this search algorithm is $O(MN)$.

5.1.3 Maximum Recovery Time. When more recovery time is available, additional error-recovery operations can be executed and the probability of success will be correspondingly higher. However, if excessive time is allowed for error recovery, there is increased risk that the bioassay will miss the completion-time deadline. Therefore, it is important to assign a maximum

```
Input: Module placement $MP$;
Output: Number of fluidic modules $N$ and locations of fluidic modules $LO$;
 1: $fluidic\_modules := \{ \}$;
 2: $PS := getPlacementSet(MP,\ module\_type)$;
 3: while $not\ PS.empty(\ )$ do
 4:     $MP_{new} := findBestPlacement(PS)$;
 5:     $fluidic\_modules.append(MP_{new})$;
 6:     if $fluidic\_modules.size(\ ) = N$ then $break$;
 7:     else
 8:         $MP.add(MP_{new})$;
 9:         $PS := getPlacementSet(MP,\ module\_type)$;
10:     end if
11: end while
12: for $MP_{new}$ in $fluidic\_modules$ do
13:     $MP.delete(MP_{new})$;
14: end for
15: $N := fluidic\_modules.size(\ )$; $LO := fluidic\_modules$;
16: return $N$, $LO$;
```

Fig. 12. Pseudo-code for determining the number of available fluidic modules.

recovery time for the recovery procedure when an error occurs in an operation. Here, we utilize the scheduler from [16] to generate 20 feasible schedules for the remaining operations by varying the recovery time t_r from 1 s to 20 s. As a result, we get 20 completion times corresponding to these 20 schedules. Note that we set the upper limit of t_r to 20 seconds, since there is no significant increase in the probability of success for $t_r > 20\ s$ for the range of laboratory bio-protocol that we studied (as we illustrate in Section 6). Finally, the maximum recovery time $\hat{t}_r$ for local error recovery is equal to the maximum value of t_r that satisfies the inequality $T(t_r) \leq T_0 + \Delta T_{max}$, where T_0 is the completion time of the bioassay when no error occurs, ΔT_{max} is the maximum allowable increase in the completion time due to errors, and $T(t_r)$ denotes the completion time when t_r time is allocated for the error recovery.

We evaluate the CPU time needed for global recovery for three bioassays described in Section 6. The maximum time to generate a schedule for these bioassays is 0.05 s on an Intel Core i3 with a 3.7GHz CPU and 8GB memory; thus, generating 20 schedules requires 1 s. To speed up the search for the maximum allowable recovery time, we use binary search to generate fewer schedules and quickly find the largest value of t_r that leads to an admissible schedule.

5.2 Online Synthesis

We now describe how online synthesis can be used to integrate local error recovery with global error recovery, as shown in Figure 13. When a bioassay is mapped to the biochip, the completion-time deadline is also specified by the user. If errors occur, the completion time of the bioassay will be larger than T_0, so we use $T_0 + \Delta T_{max}$ as an upper bound on the acceptable completion time. If the completion time T satisfies the condition $T \leq T_0 + \Delta T_{max}$, the bioassay is deemed to be successful; otherwise, it fails.

We first generate an initial schedule and module placement. All operations are stored in the operation queue in ascending order of start times and retrieved sequentially. Before executing new operations, the controller of the MEDA biochip examines the status of all on-going local error recoveries and: (1) if any local error-recovery procedure fails (e.g., the recovery time exceeds the maximum allowable recovery time), the bioassay fails; (2) if a local error recovery finishes within

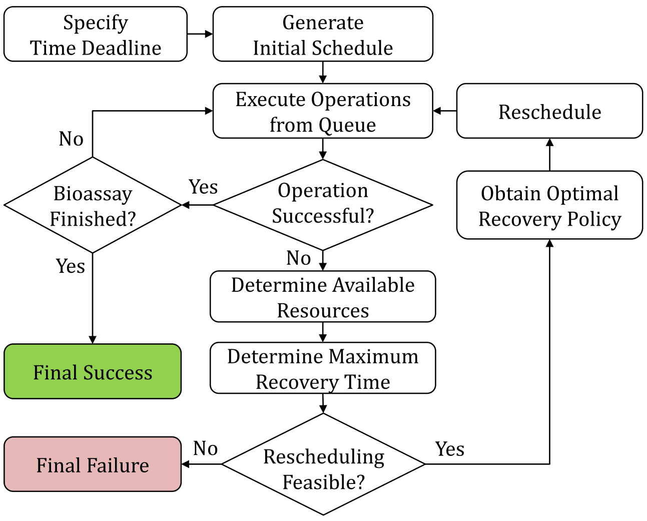
Specify Time Deadline
Generate Initial Schedule
Execute Operations from Queue
Reschedule
No
Bioassay Finished?
Yes
Operation Successful?
Obtain Optimal Recovery Policy
Yes
No
Determine Available Resources
Final Success
Determine Maximum Recovery Time
Final Failure
No
Rescheduling Feasible?
Yes

Fig. 13. Online synthesis for global error recovery.

the maximum allowed recovery time, the schedule and module placement will be updated to carry out the remaining operations as soon as possible.

Following this step, the controller on the MEDA biochip checks if there is any new error. If a new error occurs, the controller determines the resources and time available for recovery from that error, and obtain the optimal error-recovery policy generated by the techniques described in Section 4. Note that *these error-recovery policies are obtained offline (i.e., at design time) and stored in a lookup table, and therefore no time is required for their computation at runtime.* To accommodate the obtained optimal error-recovery policy, the schedule is updated appropriately.

6 EXPERIMENTAL RESULTS

In this section, we first evaluate our local error-recovery approach by focusing on the composed model from Section 4. Next, we demonstrate the effectiveness of our global error-recovery technique by presenting results of simulating our technique on three representative real-life bioassays. Finally, using the same benchmarks, we compare our approach with the static protocol proposed in [15], since the latter significantly outperforms other existing methods.

6.1 Model Analysis

Since the optimal synthesized strategy π^* resolves the nondeterminism of *erp*, the resulting game $\mathcal{G}^{\pi^*}$ is reduced to an MDP where *platform* controls the available resources. For a specific strategy σ of *platform*, the game $\mathcal{G}^{\pi^*,\sigma}$ is reduced to a DTMC. Thus, we use the induced model to study the system under the optimal policy.

To understand the impact of available resources on the error-recovery process, we run experiments on $\mathcal{G}^{\pi^*,\sigma}$ where $\sigma \in \Sigma$ and Σ is a set of finite *plat* strategies constructed by choosing a finite set of values for each resource, namely

$$r_{time}^{init} \in \{0:2:20\},\ r_{mix}^{init} \in \{0:1:4\},\ r_{cbu}^{init} \in \{0,1\}. \tag{1}$$

We can then obtain the expected success probability p_{max} under the optimal policy π^* and all possible initial sets of available resources $(r_{time}^{init}, r_{mix}^{init}, r_{cbu}^{init})$. We formally describe the query as

$$p_{max=?}^{\pi^*,\sigma}\ [\ \lozenge\ Succeed\ ] \qquad \forall \sigma \in \Sigma. \tag{2}$$

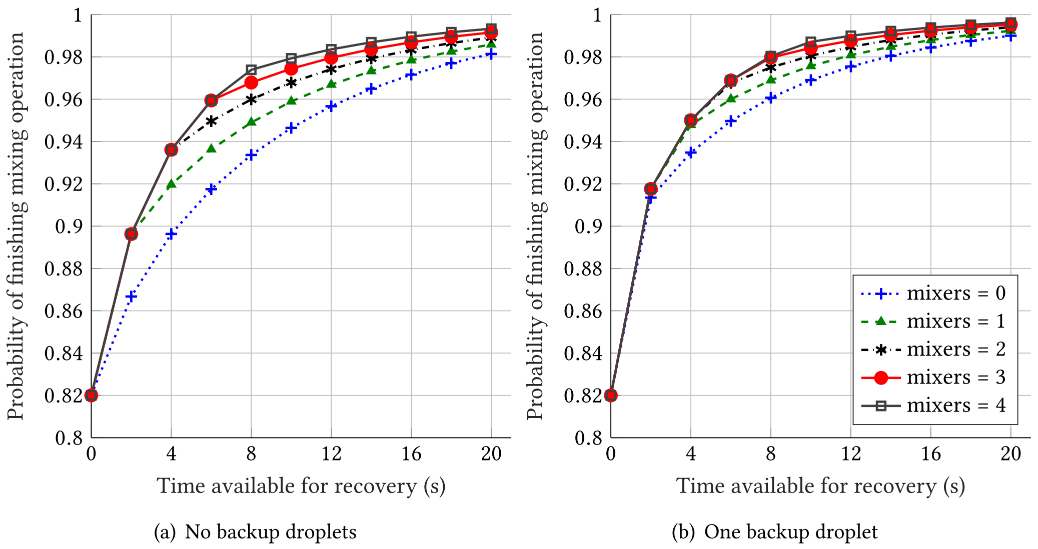

Fig. 14. Effect of resource availability for a mixing operation on its success probability under the optimal error-recovery protocol.

The computational complexity of solving (2) is $O(N_t^3 N_m^3 N_c^3)$, where N_t, N_m and N_c are the number of values for time units, mixers, and backup droplets, respectively (e.g., 11, 5 and 2 in (1)). For the set of initial resources from (1), PRISM-games solved the query and computed the optimal local error-recovery policy in 2.68s on an Intel Core i7 4.0GHz CPU. Recall that this computation is performed only once offline. Figure 14 shows the obtained results, illustrating the effect of resource availability on the probability that a mixing operation is successfully performed under the optimal error-recovery protocol. The general trend shows that the more the resources available, the higher the success probability is. Since the mixing process takes 2s to complete, time increments of 1s do not result in change in probabilities. With the same available amount of time, the improvement in probabilities between having (0 mixers, 0 droplets) and (3 mixers, 1 droplet) peaks when the time is at least 4s (5.38%) then takes a downward trend as time is increased. The combination (4s, 2 mixers, 1 droplet) has the lowest time required to guarantee a success probability of at least 95%. If more time is afforded, (6s, 2 mixers, 0 droplets) can guarantee approximately the same probability.

6.2 Benefits of the Dynamic Protocol

One significant advantage of our proposed dynamic recovery protocol over the static one from [15] is the higher probability to recover from erroneous operations, especially those residing on the side branches of a sequencing graph. The reason is that a static protocol follows a fixed policy to recover from erroneous operations, failing to exploit the variance of time and other on-chip resources. On the other hand, a dynamic protocol generates the optimal recovery policy based on the currently available resources. To illustrate this, consider the bioassay protocol shown in Figure 15, which has a long critical path (from D_1 to S_4) and a long side branch path (from D_8 to M_5). The schedule of this particular bioassay when no error happens is shown in Figure 16(a). Here, the completion-time deadline is 24s, which means the maximum allowed completion time increment Δt_{max} is 2s. We discuss the following two cases:

(1) If an error occurs in the critical path (e.g., in M_4). As shown in Figure 16(b), the maximum recovery time $\hat{t}_r$ for both the static and dynamic protocols is 2s. Within this period of

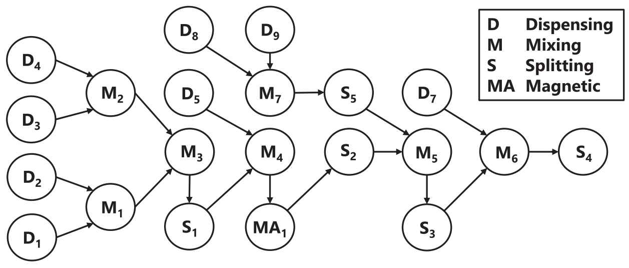

Fig. 15. The sequencing graph of an example bioassay.

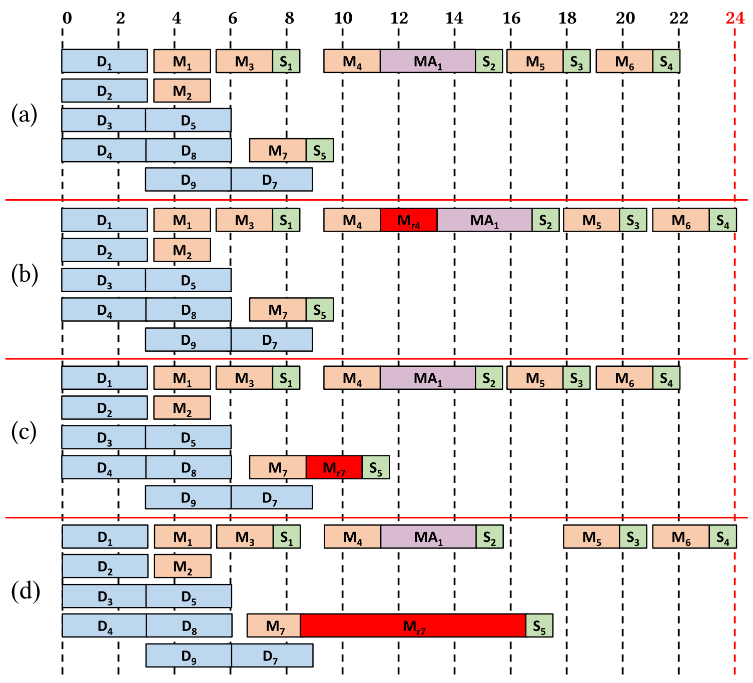

Fig. 16. The schedule when error (a) never occurs, (b) occurs in M_4, (c) occurs in M_7 using static protocol, (d) occurs in M_7 using dynamic protocol.

time, the probability of success for local recovery is 0.3 and 0.57 for the static and dynamic protocols, respectively.

(2) If an error occurs in the side branch path (e.g., in M_7). Since the static protocol relies on a fixed policy, as shown in Figure 16(c), the maximum recovery time for M_7 to recover from an error is 2s, and the probability of success for error recovery remains 0.3. However, the dynamic protocol examines the available time and other on-chip resources for error recovery and generate the optimal error-recovery policy. Figure 16(d) shows that 8s are used to recover M_7, and the probability of success for error recovery significantly increases to 0.9.

6.3 Results for Bioassays

We evaluated the proposed global error-recovery method on three real-life benchmarks shown in Figure 17, namely CEP, master-mix, and serial-dilution [9]. CEP is a combination of three small bioassays: cell lysis, mRNA extraction and mRNA purification. The experimentally characterized

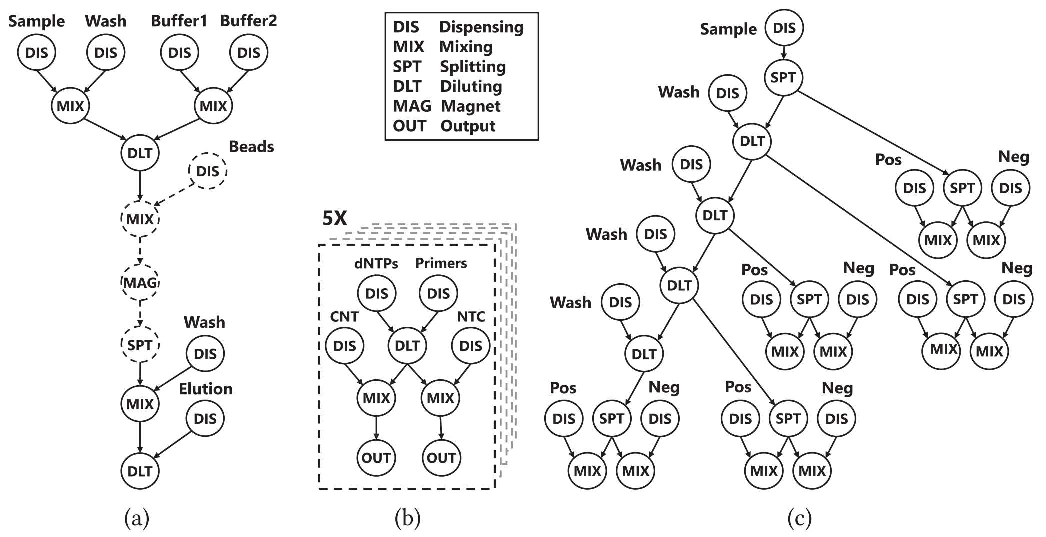

Fig. 17. (a) CEP benchmark. (b) Master-mix benchmark. (c) Serial-dilution benchmark.

module library for MEDA is presented in [15]. The size of one electrode in a conventional DMFB is equal to a 4×4 microelectrode array in MEDA biochips. Therefore, a 2×2 array in the MEDA platform actually represents an 8×8 microelectrode array. We then set the chip size to be an 8×8 array.

The error-recovery capability of a MEDA-based biochip can be evaluated based on both the bioassay completion time and probability of success (POS) when errors are detected. In our simulation, we randomly inject up to four errors into each benchmark and simulate 1000 execution scenarios under each configuration. Then, we calculate the average completion time and probability of success under different Δt_{max}, where Δt_{max} denotes the maximum allowed bioassay completion time increment. For example, if Δt_{max} is set to 10s and the completion time for a bioassay without errors is 20s, then the bioassay completion-time deadline is 30s.

As shown in Figure 18, a larger Δt_{max} and a smaller number of inserted errors result in higher probability of success for all three bioassays. Nevertheless, this comes at the cost of a slight increase in the completion time. Therefore, a trade-off between the completion time and the probability of success exists.

To compare the proposed dynamic protocol with the static one from [15], we simulate 1000 times per each number of errors from one to four, where the location at which the errors are injected is randomized. We compare the completion time under the same probability of success, as well as the probability of success under different ΔT_{max} — the results for both protocols are shown in Figure 19. When only one error occurs, the dynamic protocol shows modest improvement. However, when two or more errors occur, it significantly outperforms the static protocol. Finally, from the experimental data presented in Section 2.1, the probabilities of two or more errors occurring in the CEP, master-mix, and serial-dilution benchmarks are 0.625, 0.947, and 0.986, respectively, highlighting the need to employ the proposed dynamic error-recovery protocol.

7 DISCUSSION AND CONCLUSION

We have presented the first work that can automatically synthesize optimal error-recovery protocols for MEDA biochips. We first model the error-recovery procedure using Markov Decision Processes (MDPs). Along with the abstract model for the platform, we obtain a stochastic multi-player

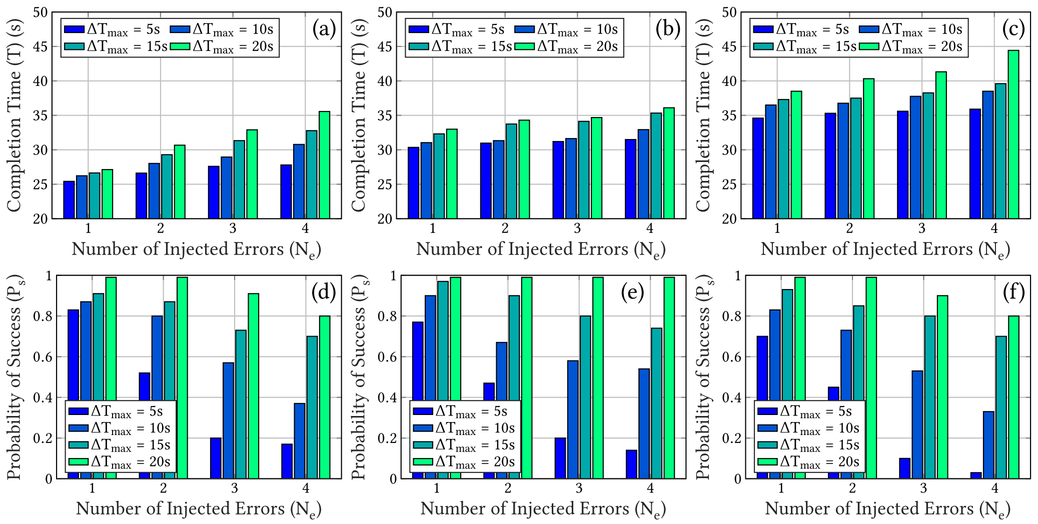

Fig. 18. The average completion time using the proposed dynamic error-recovery protocol for (a) CEP, (b) master-mix, and (c) serial-dilution; the probability of success for (d) CEP, (e) master-mix, and (f) serial-dilution.

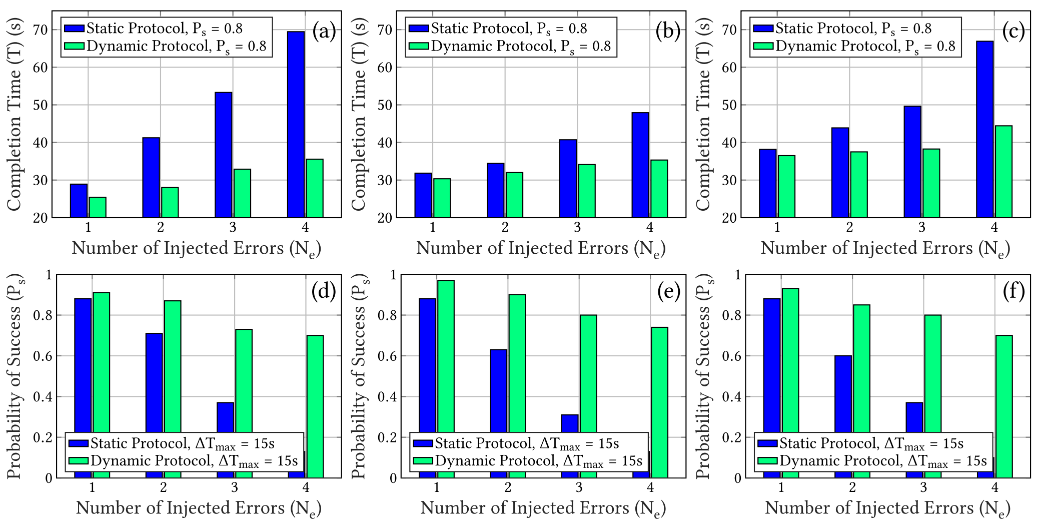

Fig. 19. A comparison between the average completion time of the static protocol from [15] and the proposed dynamic protocol for (a) CEP, (b) master-mix, (c) serial-dilution; and their POS for (d) CEP, (e) master-mix, and (f) serial-dilution.

game (SMG)-based system model. We then formalize the error-recovery procedure objectives and use them to generate optimal error-recovery protocols for local recovery. We also propose a global-recovery technique to dynamically (i) assign resources for local recovery and (ii) generate new synthesis results, i.e., operation-scheduling and module-placement results. Although the local recovery plans are optimal, the global scheduling policy is based on heuristics. As part of future work we will focus on deriving more efficient scheduling algorithms. Finally, simulation results from three real-life bioassays demonstrate the effectiveness of the proposed error-recovery technique.

As a biochip ages, the probability that an error occurs in a fluidic operation is more likely to increase over time. Hence, future work can extend the model such that the probability distribution over possible outcomes is dynamically updated, potentially by gathering statistical data from the biochip. In that case, online protocol synthesis can be useful to realize such implementation.

Furthermore, the life of a biochip can be prolonged if less error-recovery operations are executed. The objective of the error-recovery protocol can then be relaxed such that, in the early stages of a bioassay, a number of minor errors are tolerated before performing any local error-recovery attempt. Thus, a balance between minimizing the time required to complete a bioassay and extending the life of the biochip can be achieved.

REFERENCES

[1] Christel Baier, Joost-Pieter Katoen, and Kim Guldstrand Larsen. 2008. *Principles of Model Checking*. MIT press.

[2] Irena Barbulovic-Nad, Hao Yang, Philip S. Park, and Aaron R. Wheeler. 2008. Digital microfluidics for cell-based assays. *Lab on a Chip* 8 (2008), 519–526.

[3] Taolue Chen, Vojtěch Forejt, Marta Kwiatkowska, David Parker, and Aistis Simaitis. 2013. Automatic verification of competitive stochastic systems. *Formal Methods in System Design* 43, 1 (2013), 61–92.

[4] Taolue Chen, Vojtěch Forejt, Marta Kwiatkowska, David Parker, and Aistis Simaitis. 2013. PRISM-games: A model checker for stochastic multi-player games. In *International Conference on Tools and Algorithms for the Construction and Analysis of Systems*. Springer, 185–191.

[5] Antonis I. Drygiannakis, Athanasios G. Papathanasiou, and Andreas G. Boudouvis. 2008. On the connection between dielectric breakdown strength, trapping of charge, and contact angle saturation in electrowetting. *Langmuir* 25 (2008), 147–152.

[6] Richard B. Fair, Andrey Khlystov, Tina D. Tailor, Vladislav Ivanov, Randall D. Evans, Vijay Srinivasan, Vamsee K. Pamula, Michael G. Pollack, Peter B. Griffin, and Jack Zhou. 2007. Chemical and biological applications of digital-microfluidic devices. *IEEE Design & Test of Computers* 24 (2007), 10–24.

[7] Yingchieh Ho, Gary Wang, Kelvin Yi-Tse Lai, Yi-Wen Lu, Keng-Ming Liu, Yun-Ming Wang, and Chen-Yi Lee. 2016. Design of a micro-electrode cell for programmable lab-on-CMOS platform. In *Proceedings of the IEEE International Symposium on Circuits and Systems*. 2871–2874.

[8] Mohamed Ibrahim and Krishnendu Chakrabarty. 2015. Efficient error recovery in cyberphysical digital-microfluidic biochips. *IEEE Transactions on Multi-Scale Computing Systems* 1 (2015), 46–58.

[9] Mohamed Ibrahim, Krishnendu Chakrabarty, and Kristin Scott. 2017. Synthesis of cyberphysical digital-microfluidic biochips for real-time quantitative analysis. *IEEE Transactions on Computer-Aided Design of Integrated Circuits and Systems* 36, 5 (May 2017), 733–746.

[10] Mohamed Ibrahim, Zipeng Li, and Krishnendu Chakrabarty. 2015. Advances in design automation techniques for digital-microfluidic biochips. In *Formal Modeling and Verification of Cyber-Physical Systems*. 190–223.

[11] Christopher Jaress, Philip Brisk, and Daniel Grissom. 2015. Rapid online fault recovery for cyber-physical digital microfluidic biochips. In *2015 IEEE 33rd VLSI Test Symposium (VTS)*. 1–6.

[12] Kelvin Yi-Tse Lai, Ming-Feng Shiu, Yi-Wen Lu, Yingchieh Ho, Yu-Chi Kao, Yu-Tao Yang, Gary Wang, Keng-Ming Liu, Hsie-Chia Chang, and Chen-Yi Lee. 2015. A field-programmable lab-on-a-chip with built-in self-test circuit and low-power sensor-fusion solution in 0.35 μm standard CMOS process. In *Proceedings of the IEEE Asian Solid-State Circuits Conference*. 1–4.

[13] Kelvin Yi-Tse Lai, Yu-Tao Yang, and Chen-Yi Lee. 2015. An intelligent digital microfluidic processor for biomedical detection. *Journal of Signal Processing Systems* 78 (2015), 85–93.

[14] Zipeng Li, Kelvin Yi-Tse Lai, Po-Hsien Yu, Krishnendu Chakrabarty, Tsung-Yi Ho, and Chen-Yi Lee. 2017. Droplet size-aware high-level synthesis for micro-electrode-dot-array digital microfluidic biochips. *IEEE Transactions on Biomedical Circuits and Systems* 11, 3 (June 2017), 612–626.

[15] Zipeng Li, Kelvin Yi-Tse Lai, Po-Hsien Yu, Krishnendu Chakrabarty, Miroslav Pajic, Tsung-Yi Ho, and Chen-Yi Lee. 2016. Error recovery in a micro-electrode-dot-array digital microfluidic biochip. In *Proceedings of the IEEE/ACM International Conference on Computer-Aided Design*. 105:1–105:8.

[16] Zipeng Li, Kelvin Yi-Tse Lai, Po-Hsien Yu, Tsung-Yi Ho, Krishnendu Chakrabarty, and Chen-Yi Lee. 2016. High-level synthesis for micro-electrode-dot-array digital microfluidic biochips. In *2016 53nd ACM/EDAC/IEEE Design Automation Conference (DAC)*. 146:1–146:6.

[17] Yan Luo, Krishnendu Chakrabarty, and Tsung-Yi Ho. 2013. Error recovery in cyberphysical digital microfluidic biochips. *IEEE Transactions on Computer-Aided Design of Integrated Circuits and Systems* 32 (2013), 59–72.

[18] Haig Norian, Ryan M. Field, Ioannis Kymissis, and Kenneth L. Shepard. 2014. An integrated CMOS quantitative-polymerase-chain-reaction lab-on-chip for point-of-care diagnostics. *Lab on a Chip* 14, 20 (2014), 4076–4084.

[19] Martin L. Puterman. 2014. *Markov Decision Processes: Discrete Stochastic Dynamic Programming.* John Wiley & Sons.

[20] Ramakrishna Sista, Zhishan Hua, Prasanna Thwar, Arjun Sudarsan, Vijay Srinivasan, Allen Eckhardt, Michael Pollack, and Vamsee Pamula. 2008. Development of a digital microfluidic platform for point of care testing. *Lab on a Chip* 8 (2008), 2091–2104.

[21] Vijay Srinivasan, Vamsee K. Pamula, Phil Paik, and Richard B. Fair. 2004. Protein stamping for MALDI mass spectrometry using an electrowetting-based microfluidic platform. *Proc. SPIE* 5591 (2004), 26–32.

[22] Mária Svoreňová and Marta Kwiatkowska. 2016. Quantitative verification and strategy synthesis for stochastic games. *European Journal of Control* 30 (2016), 15–30.

[23] Erin R. Ferguson Welch, Yan-You Lin, Andrew Madison, and Richard B. Fair. 2011. Picoliter DNA sequencing chemistry on an electrowetting-based digital microfluidic platform. *Biotechnology Journal* 6 (2011), 165–176.

[24] Yang Zhao, Tao Xu, and Krishnendu Chakrabarty. 2010. Integrated control-path design and error recovery in the synthesis of digital microfluidic lab-on-chip. *ACM Journal on Emerging Technologies in Computing Systems* 6, 3, Article 11 (Aug. 2010), 28 pages.

Received April 2017; revised May 2017; accepted June 2017